

Integrating visual cues for motor control: A matter of time

Hal S. Greenwald *, David C. Knill, Jeffrey A. Saunders

Center for Visual Science, University of Rochester, 274 Meliora Hall, Box 270270, Rochester, NY 14627-0270, United States

Received 23 July 2004; received in revised form 10 January 2005

Abstract

The visual system continuously integrates multiple sensory cues to help plan and control everyday motor tasks. We quantified how subjects integrated monocular cues (contour and texture) and binocular cues (disparity and vergence) about 3D surface orientation throughout an object placement task and found that binocular cues contributed more to online control than planning. A temporal analysis of corrective responses to stimulus perturbations revealed that the visuomotor system processes binocular cues faster than monocular cues. This suggests that binocular cues dominated online control because they were available sooner, thus affecting a larger proportion of the movement. This was consistent with our finding that the relative influence of binocular information was higher for short-duration movements than long-duration movements. A motor control model that optimally integrates cues with different delays accounts for our findings and shows that cue integration for motor control depends in part on the time course of cue processing.

© 2005 Elsevier Ltd. All rights reserved.

Keywords: Visuomotor integration; Monocular; Binocular; Stereopsis; Temporal dynamics; Cue processing; Cue integration; Motor planning; Online control

1. Introduction

The past decade has been a period of intense research focused on understanding how the brain integrates three-dimensional information about the world from different sensory cues (Ernst & Banks, 2002; Hillis, Ernst, Banks, & Landy, 2002; Jacobs, 1999; Knill & Saunders, 2003; Landy, Maloney, Johnston, & Young, 1995; Saunders & Knill, 2001). Existing studies have focused almost exclusively on perceptual judgments of 3D object properties, but the primary reason for producing accurate estimates of these properties is to control motor behavior. Picking up an object, putting an object on a surface, and hammering a nail are all examples of everyday motor behaviors that require integrating informa-

tion from multiple cues to generate accurate visual estimates of object size, shape, position, and orientation.

A central issue in sensory processing as it pertains to motor control is how the brain accumulates and uses sensory information over time. Perceptual studies of cue integration, largely because they rely on discrete judgments, have treated sensory estimation as a static process. Goal-directed hand movements, however, occur over time spans that are sufficiently short (typically less than a second) for the temporal properties of cue integration to impact how different cues contribute to the control of motor acts. How the brain integrates visual information over time significantly impacts the roles that different cues play in online control.

Previous results have shown that monocular cues provided by texture and the outline shapes of figures can be as reliable as or more reliable than binocular cues to 3D surface orientation (Hillis, Watt, Landy, & Banks, 2004; Knill & Saunders, 2003; Saunders & Knill, 2001).

* Corresponding author. Tel.: +1 585 275 3322; fax: +1 585 271 3043.
E-mail addresses: hgreenwald@bcs.rochester.edu (H.S. Greenwald), knill@cvs.rochester.edu (D.C. Knill).

Moreover, subjects are almost as accurate at orienting an object for placement on a slanted surface when such cues are presented monocularly as when they are presented binocularly (Knill & Kersten, 2004). We therefore used an object placement task to assess how the brain integrates binocular and monocular cues to 3D

surface orientation for visuomotor control. Fig. 1 illustrates the task and the experimental apparatus.

Following on suggestions that the visual processes mediating motor planning are distinct from those that subserve online control of movements (Glover & Dixon, 2001, 2002), we measured the relative contributions of

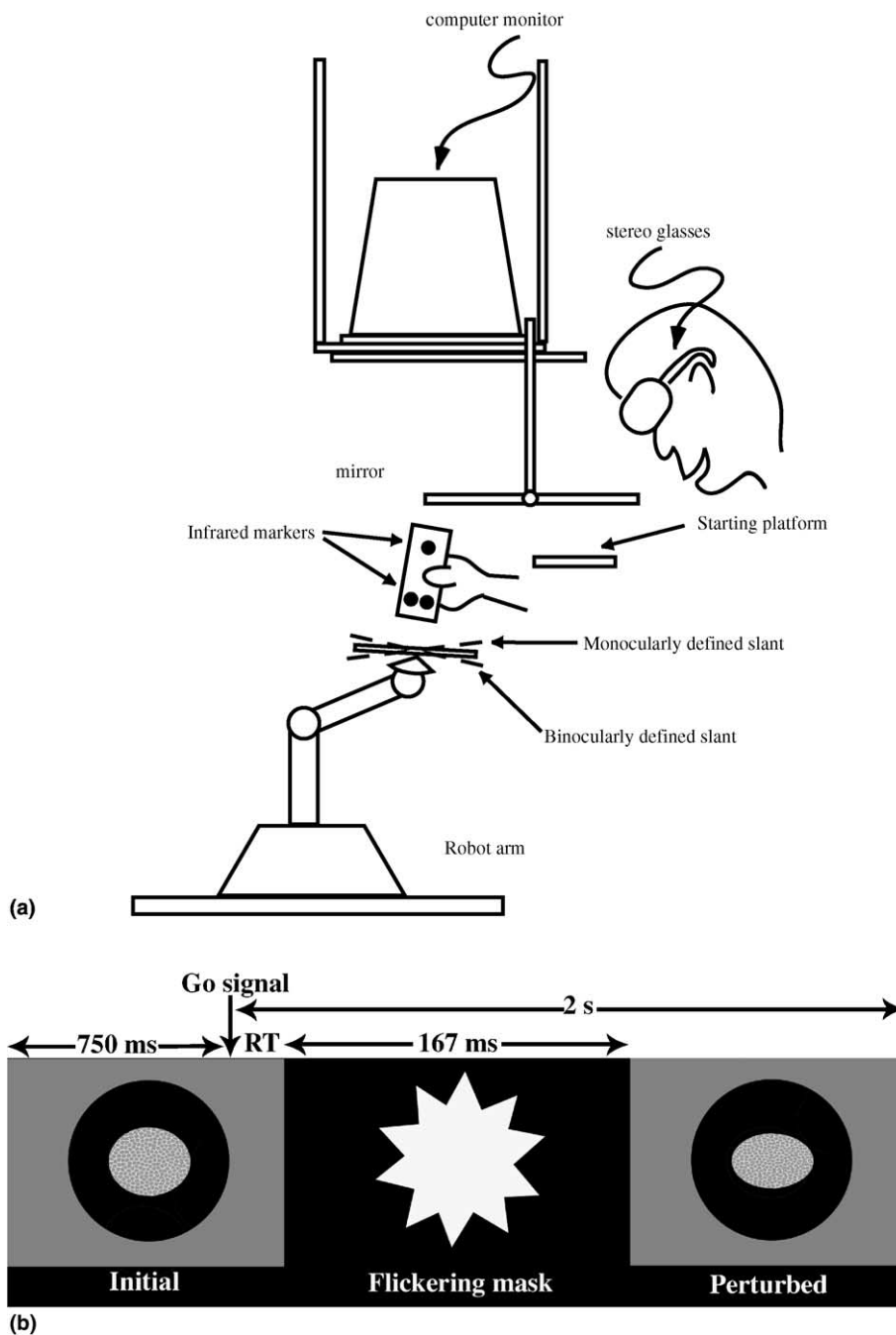


Fig. 1. (a) The experimental setup (see text for description). The surface appears here with a 35° slant. In Experiment 1, the visual cues were consistent with each other and the physical surface. In Experiment 2, conflicts between monocular and binocular cues were no more than half the size shown here. (b) The task sequence. The surface was displayed for 750 ms prior to the go signal and remained until subjects picked up the cylinder (reaction time). Movement initiation caused the screen to alternate between black and white every other frame for 167 ms. After the flickering mask ended, the surface reappeared and remained until 2 s had elapsed since the go signal. On some trials, the surface slant was perturbed by $\pm 5^\circ$. The perturbation shown here is exaggerated for illustration purposes. Movement duration was the elapsed time between when subjects removed the cylinder from the starting surface and when it first contacted the target surface.

binocular and monocular depth cues to both planning and online control of the simple reaching movements used for object placement. We found that binocular cues influence online control more than planning. This led us to analyze the temporal evolution of subjects' corrective movements in response to independent perturbations in the cues as a means to understand the temporal dynamics of the cue integration process during the online control phase of movements. The results show that differences in the speed with which binocular and monocular cues are processed account for the apparent differences in how cues contribute to planning and online control. We describe a model that generalizes static statistical models of cue integration to a dynamic process that integrates sensory information continuously over time in a statistically optimal way. By simulating qualitatively different forms of the model, we show that the empirical results obtained here cannot be accounted for by a simple difference in cue reliability but require the existence of temporal differences in cue processing. The model shows how the contribution of different sensory cues to motor behavior results from the interplay between temporal constraints in visual processing and the intrinsic reliability of cues.

2. Experiment 1

The first experiment tested whether subjects continuously used visual information about the orientation of the target surface to control their movements when placing a cylinder on it. Previous studies have shown that subjects correct for the position of a stimulus when it is altered during a movement, even when they are perceptually unaware of the perturbation (e.g. by perturbing the position during an orienting saccade to the target)¹ (Goodale, Pelisson, & Prablanc, 1986; Pelisson, Prablanc, Goodale, & Jeannerod, 1986; Prablanc & Martin, 1992; Soechting & Lacquaniti, 1983). We used a similar strategy to test for online corrections in response to changes in visual information about surface orientation occurring during reaching. To mask the motion transients created by the perturbations, we flickered the display for 10 video frames at the time of the perturbation. The closest natural analog to this would be an eye blink. No subjects reported noticing the perturbations, even when told about them explicitly after the experiment.

¹ Other studies have shown that subjects make online corrections for changes in the size and orientation of an object; however, these changes were accompanied by highly salient, detectable transients in the visual stimulus. It is not clear whether or not subjects use visual information about these object properties to make online corrections to their grip and hand posture in the absence of such transients.

2.1. Methods

2.1.1. Apparatus

Participants viewed a 20 in. computer monitor through a horizontal half-silvered mirror so that the virtual image of the monitor appeared as a horizontal surface behind the mirror (see Fig. 1a). An opaque backing placed underneath the mirror during experimental trials prevented subjects from seeing anything but the image on the monitor. Images were displayed at a resolution of 1152×864 pixels resolution at a 118 Hz refresh rate in stereo mode (59 Hz refresh rate for each eye) through Crystal Eyes stereo goggles. Subjects sat with their head in a chin rest that oriented their view down towards the mirror. They viewed the computer-rendered images through circular occluders positioned in front of each eye to prevent vision outside the central area of the workspace; the edges of the computer monitor were never visible.

Subjects viewed a circular, textured surface in a stereoscopic virtual display and were asked to place a cylinder flush onto the surface; a robot arm placed a real surface co-aligned with the virtual surface so that subjects actually were placing the cylinder onto a real surface. The disk was randomly presented at a range of slants relative to the viewer (the angle of the surface away from the fronto-parallel) ranging from 15° (near fronto-parallel) to 45° (in our setup, slightly more slanted than a horizontal tabletop).

A PUMA 260 robot arm positioned a round metal target plate in the workspace below the monitor to be co-aligned with the virtual surface. On each trial, subjects moved a plexiglass cylinder measuring 6.4 cm in diameter and 12.7 cm in height and weighing 227 g from a starting plate located to the right of the subject to the target surface. An Optotrak 3020 system (Northern Digital, Inc.) tracked the 3D positions of four infrared markers placed on the cylinder at 120 Hz.

A metal plate mounted on the bottom of the cylinder was connected to a 5 V source, and both the starting plate and the target plate on the end of the robot arm were connected to a Northern Digital Optotrak Data Acquisition Unit II. The data acquisition unit recorded the voltage across each plate so that a 5 V signal indicated when a plate was in contact with the cylinder's metal base. The signals on each plate were recorded at 120 Hz and were used to mark the beginning of a movement and the time of initial contact between the cylinder and the target surface.

2.1.2. Calibration procedures

Spatial calibration of the virtual environment required computing the coordinate transformation from the reference frame of the Optotrak to the reference frame of the computer monitor and the location of a subject's eyes relative to the monitor. These parameters

were measured at the start of each experimental session using an optical matching procedure. The backing of the half-silvered mirror was temporarily removed so that subjects could see their hand and the monitor simultaneously, and subjects positioned an Optotrak marker at a series of visually cued locations. Cues were presented monocularly, and matches were performed separately for both eyes. Thirteen positions on the monitor were cued, and each position was matched twice at different depth planes. We calculated the three-dimensional position of each eye relative to the center of the screen by minimizing the squared error between the settings for the probe predicted by the eye position and the measured probe settings. After the calibration procedure, a rough test was performed in which subjects moved a marker viewed through the half-silvered mirror and checked that a dot rendered binocularly appeared co-aligned with the marker.

Another calibration procedure determined the coordinate transformations between the Optotrak reference frame and the reference frame of the robot arm. An infrared marker was placed on the end of the robot arm. We then moved the robot arm along each of its three coordinate axes and measured the resulting displacement of the marker in Optotrak coordinates. The transformations computed from this and the viewer calibration procedure allowed us to position the physical target surface in the same location and orientation relative to a subject as the virtual target surface used for the stimulus.

2.1.3. Stimuli

Target surfaces were rendered as circles filled with randomly generated Voronoi textures (see Fig. 1b). The elliptical outlines of the surfaces and the texture patterns provided monocular cues about target orientation. Disparity between the features in the images presented to the two eyes provided binocular information.² Stimuli were drawn in red to take advantage of the comparatively faster red phosphor of the monitor and prevent inter-ocular cross-talk. The Optotrak data was used in real-time to compute the position and orientation of the cylinder and to render the cylinder when it appeared in the workspace below the monitor. Subjects only saw the rendered cylinder during the 250–300 ms prior to target contact when it appeared within the circular apertures through which they viewed the scene. We used a linear extrapolation routine that accounted for the temporal delay (~25 ms) between the Optotrak recording and the display of the cylinder, so the cylinder always appeared at the correct location and orientation.

² Motion cues were eliminated by use of a chin rest. Blur and accommodation cues were determined by the orientation of the screen. Those cues always conflicted with disparity and figural cues manipulated in the experiment.

When viewed through a half-silvered mirror, differences between the pose of the real and virtual cylinder were only apparent at the very end of a movement, when the cylinder decelerated sharply at contact.

The target surface was presented 35 cm in front of the observer and 45 cm below their eyes. When horizontal, the target surface would have appeared at a 38° slant relative to the observer's line of sight to the center of the surface. Relative to the target surface, the starting plate was positioned 40 cm to the right, 20 cm closer to the observer, and 10 cm higher.

2.1.4. Procedure

Subjects participated in two 1-h sessions, each consisting of four 80-trial blocks. Practice trials were administered at the start of the first session until the subject understood the task and could perform it correctly. On each trial, the virtual target surface was displayed at a slant ranging from 15° to 45° in 5° increments. After displaying the surface for 750 ms, the computer produced an audible signal to tell subjects to begin moving the cylinder from the starting plate to the target plate. Upon movement initiation, the screen flickered black and white for 10 display frames (167 ms) before the stimulus reappeared (see Fig. 1b). On 36% of trials, the slant of the target surface changed by $\pm 5^\circ$ after the flickering mask. These stimulus perturbations were limited to trials on which the initial target surface slant was either 25° or 35°. The flicker masked the motion transient caused by the change in surface slant. No subjects reported noticing the changes in orientation, even when told afterward about the perturbations. Each trial ended when the cylinder contacted the target plate, which provided subjects with haptic feedback about the target slant. Trials not completed within 2 s after the go signal were discarded.

2.1.5. Subjects

The eight participants in this experiment were from the University of Rochester community, had normal or corrected-to-normal vision, reported having normal binocular vision, were right handed, and were naïve to the purposes of the study. Written informed consent was obtained from each volunteer, and subjects were paid \$10 per hour for their participation. The experiments were conducted according to the guidelines set by the University of Rochester Research Subjects Review Board, who approved the study.

2.2. Results

Fig. 2a shows the mean cylinder trajectories for one subject. For unperturbed trials, the subject continuously adjusted the orientation of the cylinder to match the target surface orientation at contact. On perturbed trials, the cylinder trajectories were initially the same as for

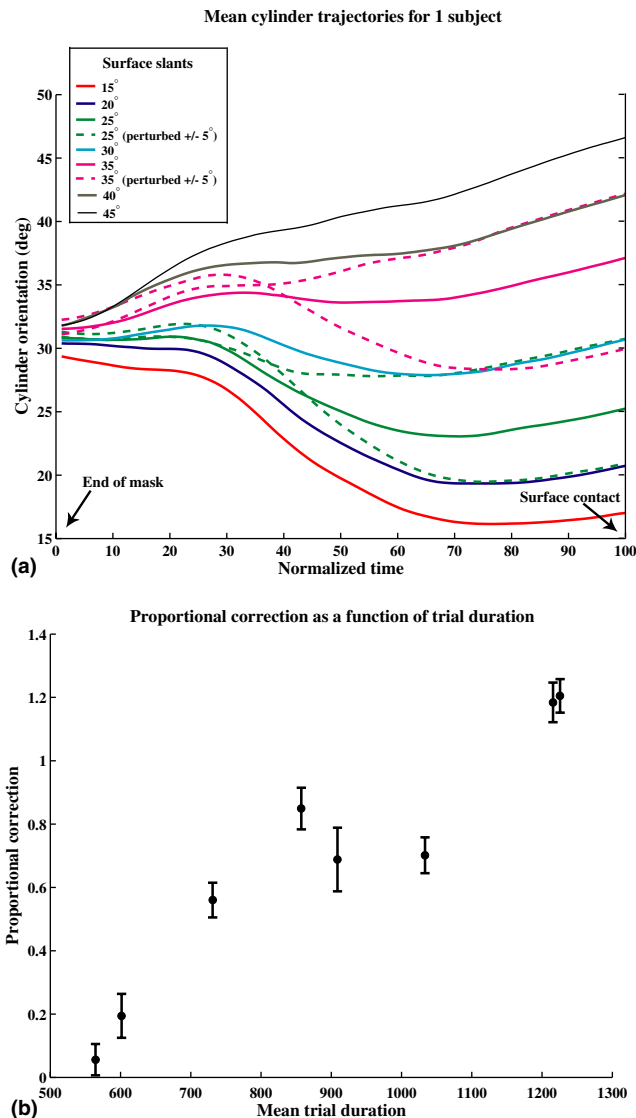


Fig. 2. (a) Mean cylinder orientation over time for 1 subject. The trajectories have been normalized so that time 0 is the end of the mask, when any perturbations would be inserted, and time 100 is when the cylinder first comes into contact with the surface. The solid lines correspond to unperturbed trials, and the dashed lines represent perturbed trials. Perturbations occurred around 25° and 35°. This subject completely corrected for the perturbations despite being unaware of them. (b) Proportional correction vs. duration. The average proportional correction in response to the perturbations is shown for each subject as a function of average movement duration.

unperturbed trials, but the subject clearly corrected the cylinder orientation after the perturbation to match the new surface slant despite not noticing that the orientation of the target surface had changed. The amount by which subjects corrected for the perturbations depended on the duration of their movements, with shorter movements leading to less correction than longer movements (see Fig. 2b). We tested this using a linear regression of subjects' average proportional corrections against their average movement duration (across subjects). The com-

puted slope was 0.00094, which was significant (the 95% confidence interval was [0.00077, 0.0011]). The small size of the slope was due to the large movement durations as measured in milliseconds.

For a more sensitive measure of how the perturbations affected the movements over time, we applied a novel analysis technique designed to measure the temporal evolution of sensory signals used to guide motor behavior (Saunders & Knill, 2003, 2004). The smooth cylinder trajectories allowed us to fit an autoregressive linear model to predict the slant of the cylinder at each time as a function of its slant at previous times. Correlating the residual error of this model fit with the perturbations in the sensory input on each trial provided a measure of the time course of the influence of each perturbation on subjects' movements. The model has the form,

$$s_t = w_1(t) * s_{t-1} + \dots + w_n(t) * s_{t-n} + k(t) * \Delta\sigma, \quad (1)$$

where s_t is the slant of the cylinder at time t . We computed the values of the weights and $k(t)$ using a series of linear regressions that predicted the current cylinder orientation from the previous seven frames and the target surface slant perturbations ($\Delta\sigma$), which were always -5° , 0° , or $+5^\circ$. The number of previous frames included in the regression only affected the smoothness of the resulting functions. We chose seven frames because this appeared to minimize the noise, though it is not crucial to the model's performance.

The weights ($w_f(t)$) capture the normal temporal correlations in the slant of the cylinder as subjects transported it. $k(t)$ measures the amount of the residual variance in the slant of the cylinder at time t that can be attributed to perturbations in the target surface slant. We refer to $k(t)$ as the *perturbation influence function*. Before subjects have time to respond to perturbations, $k(t)$ equals zero, and its value changes over time according to how much added influence the perturbation has on the orientation of the cylinder at time t (above and beyond its influence on earlier orientations, as propagated through the autoregressive model).

Fig. 3a shows the perturbation influence functions computed by grouping trials across all subjects for perturbations around 25° and 35°. These indicate that subjects corrected for the perturbations with approximately a 250–300 ms delay (measured from the end of the masking flicker). Fig. 3b shows individual perturbation functions from three subjects with different durations; the trends shown in Fig. 3a are reflected across individuals.

2.3. Discussion

Past studies have shown that subjects correct for changes in stimulus position, size, and orientation in

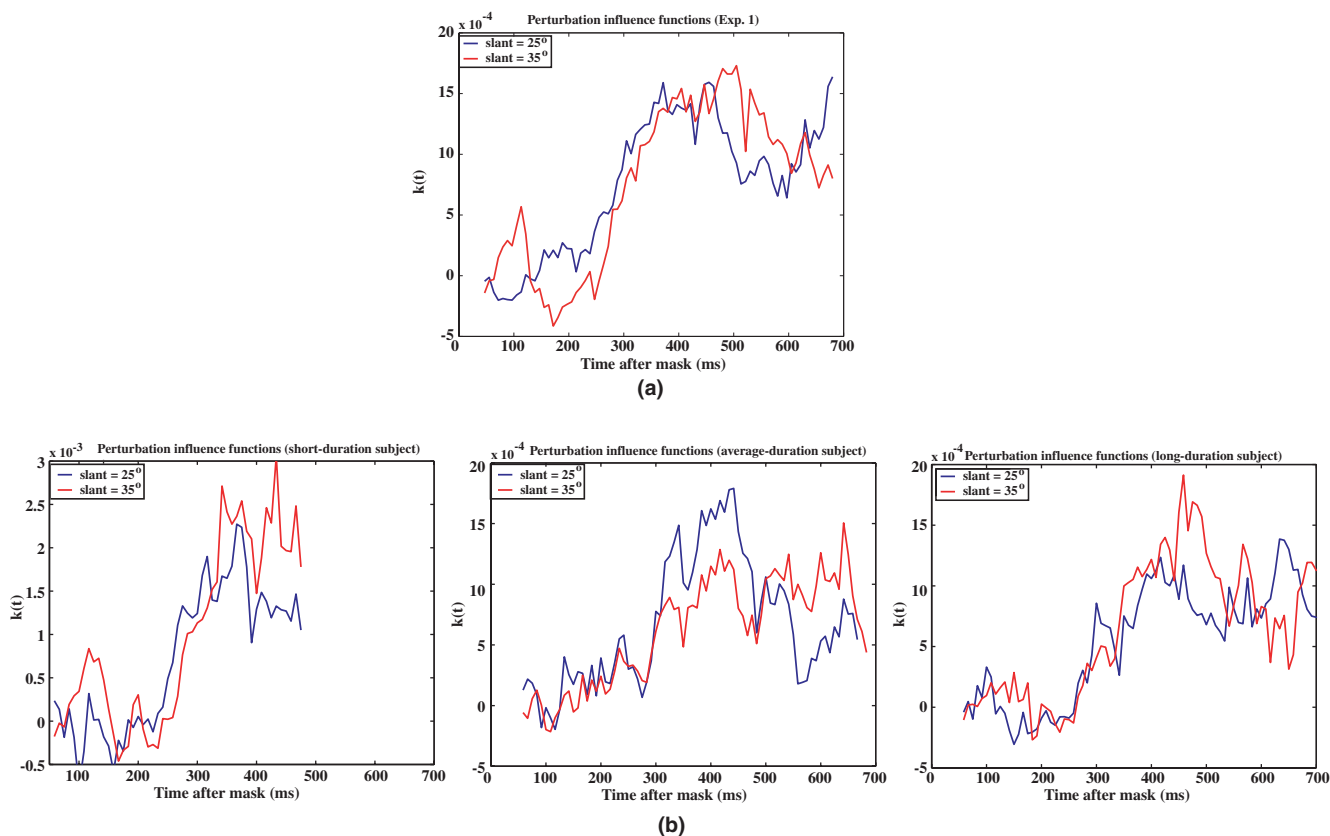


Fig. 3. (a) Perturbation influence functions for Experiment 1. Influence functions are shown for each of the slants used for perturbation trials. (b) Representative perturbation influence functions from three subjects whose movements lasted for different durations.

the frontal plane when the perturbations are detectable (Desmurget et al., 1996; Paulignan, Jeannerod, Mackenzie, & Marteniuk, 1991; Paulignan, Mackenzie, Marteniuk, & Jeannerod, 1991). Similarly, subjects correct for changes in target position even when unaware of the perturbations, like when they are masked by a saccade (Goodale et al., 1986; Prablanc & Martin, 1992). Only the latter result clearly implicates a role of visual target information in normal online control of hand movements. The current results show that orienting movements as well as hand transport are under the control of continuously updated visual estimates of three-dimensional target surface orientation. While perhaps not surprising, establishing this was a prerequisite for performing Experiment 2, which used a similar perturbation technique to measure the separate influences of monocular and binocular cues.

The reaction times we obtained from the temporal decorrelation analysis showed that responses to changes in surface slant are noticeably slower than corrections to two-dimensional target displacements, which occur within 100–150 ms (Paulignan et al., 1991; Paulignan et al., 1991; Prablanc & Martin, 1992). This may be due to the more complex processing required to estimate slant but could also reflect delays caused by the flicker used to mask the orientation perturbation.

3. Experiment 2

We quantified the relative contributions of monocular and binocular cues to task performance by providing conflicting 3D orientation information from the two cues and correlating the kinematics of subjects' movements with the orientations suggested by the individual cues. To study differences in cue integration for planning and online control of motor behavior, we introduced cue conflicts either at stimulus onset (when subjects were planning movements) or at movement onset (when subjects were executing reaching movements). Analyzing the contributions of the different cues to the movement over time revealed differences in the temporal dynamics of processing monocular and binocular information.

3.1. Methods

3.1.1. Apparatus

The apparatus was identical to that used in Experiment 1.

3.1.2. Stimuli

Target surface stimuli like those from Experiment 1 were presented at slants ranging from 20° to 45° in 5° increments. In *cue-consistent* trials, target surfaces were

rendered at the specified slant, but in *cue-conflict* trials, the binocular disparities were made to suggest a slant different from the monocular cues (the outline shape of the figure and the texture pattern). Cue-consistent stimuli were presented at the full range of slants. Cue conflicts were added only around a base slant of 35°, an angle at which subjects give significant weights to both monocular and binocular cues (Saunders & Knill, 2003), using all nine combinations of 30°, 35° and 40° for the monocular and binocular slants (three of these were cue-consistent conditions).

Cue conflicts were generated by rendering a distorted copy of the surface and texture at the slant specified for the binocular cue. The surface and texture were distorted so that when projected from the binocular slant to a point midway between a subject's eyes (the cyclopean view), the projected surface and texture suggested the slant specified for the monocular cue on that trial. To compute the appropriate distortion, we projected the positions of the surface and texture vertices into the virtual image plane of a cyclopean view of a surface with the slant specified for the monocular cue. Then, we back-projected these projected vertex positions onto a plane with the specified binocular slant to generate the new, distorted texture vertices.

In *unperturbed* cue conflict trials, the cue conflicts were present in the stimulus when it first appeared in the display, and the stimulus remained unchanged throughout the trial. In this case, the cue conflicts affected both planning and online control of movements. In the *perturbed* cue conflict conditions, the initial stimulus display had no cue conflicts (both binocular and monocular slants were set to 35°), but we added conflicts at movement onset by perturbing one or both cues using the same method described for Experiment 1. In these trials, responses to the cue conflicts could only reflect online use of visual information for controlling a movement.

To prevent subjects from learning a dependency on either cue based on the haptic feedback, the physical target surface was oriented at a slant randomly selected from a range of slants $\pm 2^\circ$ around the average slant suggested by the two cues (the random perturbation was added on both cue-consistent and cue-conflict trials).

3.1.3. Procedure

Subjects participated in four 1-h sessions, each consisting of four 80-trial blocks. Since Experiment 1 showed that subjects' corrections began approximately 275–300 ms after the end of the visual mask, we restricted movement durations to be at least 600 ms to allow sufficient time for responding to the perturbations. Most subjects required 700–1000 ms to complete a reach, so the 600 ms threshold was below the range of natural movement speeds. If subjects moved the cylinder before the go signal, completed the movement in less

than 600 ms, or did not complete the trial within 2 s after the go signal, subjects received an error message, and the trial was rerun at a random time later in the same block. Otherwise, the progression of each trial was identical to trials in Experiment 1.

3.1.4. Subjects

Nine subjects participated in this study. All met the same criteria specified for Experiment 1, and no subjects participated in both experiments.

3.2. Results

To quantify the relative overall contributions of binocular and monocular cues to a movement, we correlated the slants suggested by each cue on a trial with the slant of the cylinder at the point just prior to making contact with the target surface (its contact slant). Most subjects showed biases in their movements that reflected a tendency to orient the cylinder to the mean of the full range of slants; therefore, we included both multiplicative and additive bias terms in the regression. This gave a linear equation relating the contact slant of the cylinder to the slants suggested by each cue of the form

$$s_{\text{contact}} = k * (w_{\text{mono}} * \sigma_{\text{mono}} + w_{\text{bin}} * \sigma_{\text{bin}}) + b, \quad (2)$$

where s_{contact} is the contact slant of the cylinder, σ_{mono} and σ_{bin} are the slants suggested by the monocular and binocular cues, respectively, including any perturbations, k and b are the bias terms, and w_{mono} and w_{bin} are weights that represent the relative contributions of the two cues to the final orientation of the cylinder. Since w_{mono} and w_{bin} are constrained to sum to 1, $w_{\text{bin}} = 1$ reflects complete dependence on the binocular cues, and $w_{\text{bin}} = 0$ reflects complete dependence on the monocular cues.

Fig. 4a plots w_{bin} for the perturbed and unperturbed conflict conditions. On average, the binocular cues contributed more to the final contact slant of the cylinder in the perturbed conditions than in the unperturbed conditions ($T(8) = 2.36, p < .05$), and this effect appears consistently across subjects. Because the perturbed conditions isolated the contribution of visual information for online corrections and performance in the unperturbed conditions reflected a mixture of planning and online effects, the results indicate that binocular cues influenced subjects' online control of their movements more than they influenced movement planning.

If we assume that the contact slants of the cylinder on unperturbed trials reflect a proportional correction of the planned contact slant, we can use the weights estimated in the two conditions to calculate the relative contributions of the cues to movement planning. Specifically, we modeled the contact slant of the cylinder as a weighted mixture of cue influences on movement planning and online corrections,

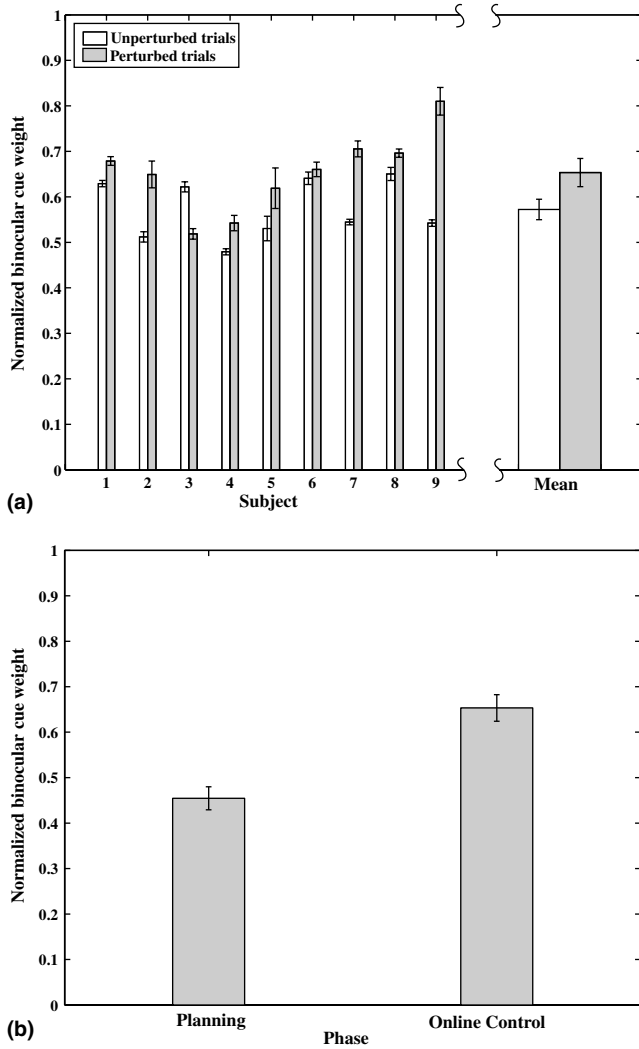


Fig. 4. (a) Normalized binocular cue weights for perturbed and unperturbed cue conflict conditions computed from the expression $w_{\text{bin}}/(w_{\text{bin}} + w_{\text{mono}})$ (a weight of 0.5 reflects equal contributions from both cues) for individual subjects and averaged across all subjects. Eight of the nine subjects relied more on binocular information for perturbed trials than for unperturbed trials. (b) Normalized binocular cue weights for planning and online control. These were inferred from the unperturbed and perturbed weights as described in the text. Since Subject 3 fully corrected for the perturbations, that subject's planning weights were unconstrained and thus were excluded.

$$s_{\text{contact}} = k_{\text{plan}} * (\pi_{\text{mono}} * \sigma_{\text{mono}} + \pi_{\text{bin}} * \sigma_{\text{bin}}) + k_{\text{online}} * (\gamma_{\text{mono}} * \sigma_{\text{mono}} + \gamma_{\text{bin}} * \sigma_{\text{bin}}) + b, \quad (3)$$

where k_{plan} and k_{online} represent the relative contributions of planning and online control to the final contact slant of the cylinder, π_{mono} and π_{bin} represent the relative contributions of monocular and binocular cues, σ_{mono} and σ_{bin} , to planning ($\pi_{\text{mono}} + \pi_{\text{bin}} = 1$), γ_{mono} and γ_{bin} represent the relative contributions of binocular and monocular cues to online control ($\gamma_{\text{mono}} + \gamma_{\text{bin}} = 1$), and b is an additive bias term. In this model,

a subject who compensates completely for planning errors during online control would have $k_{\text{plan}} = 0$, while a subject performing a ballistic movement (no online corrections) would have $k_{\text{online}} = 0$. By fitting the weights for visual cues and movement phases using linear regressions, we can infer how monocular and binocular cues contribute to planning and online control and how planning and online control contribute to visual control of reaching movements.

Fig. 4b shows the results of applying the model to the data derived from the perturbed and unperturbed conditions. The binocular weight for online control is given by the weight derived from the perturbed trials since the first term in Eq. (3) is a constant in that case (the slants suggested by binocular and monocular cues for planning were equal in these conditions). Binocular cues influenced online control more than planning by a factor of 50%.

One possible explanation for the difference is that the visual computations underlying online control are distinct from those underlying motor planning, with online visual computations giving more weight to binocular information than the computations used for planning movements. An alternative explanation, however, is that the visual computations for motor planning and online control are identical and that the differences arise from different time constants in the mechanisms that process binocular and monocular cues. In the short time available for online control, monocular cues may be processed too slowly to have as much impact on control as they have on planning, when more time is available to integrate them with binocular cues.

To test this, we applied the same temporal decorrelation analysis technique used in Experiment 1 to the cue conflict data. As in the previous experiment, we computed the influence of the perturbations using a series of linear regressions. This required expanding the influence term, $k(t)$, into two components, $k_{\text{bin}}(t)$ and $k_{\text{mono}}(t)$, one each for the perturbations in the binocular and monocular cues, $\Delta\sigma_{\text{bin}}$ and $\Delta\sigma_{\text{mono}}$, in the cue perturbation trials.

$$s_t = w_1(t) * s_{t-1} + \dots + w_n(t) * s_{t-n} + k_{\text{bin}}(t) * \Delta\sigma_{\text{bin}} + k_{\text{mono}}(t) * \Delta\sigma_{\text{mono}}. \quad (4)$$

As before, we fit the weights and values of the influence functions at each time t using linear regression. Fig. 5 shows the influence functions for the binocular and monocular cues. While the weights assigned to the monocular and binocular perturbations eventually reach the same levels, the binocular perturbation influence function increases earlier, or at least more quickly, than the monocular perturbation influence function. The relative influence of the two cues asymptotes approximately 250–300 ms after the initial response to the new information.

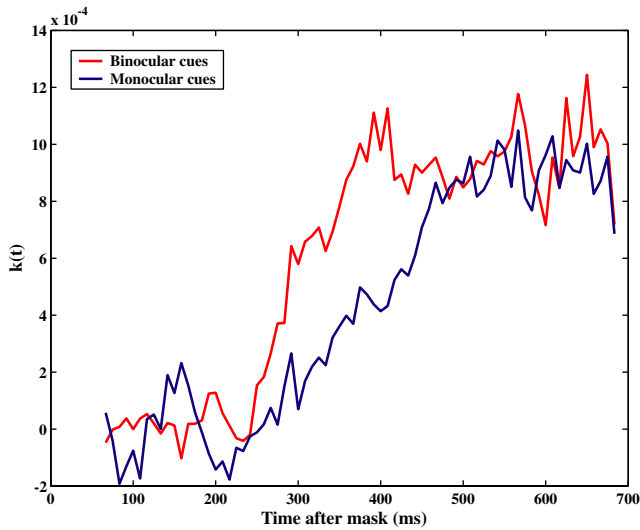


Fig. 5. Perturbation influence functions for each cue in Experiment 2, showing the separate effects of monocular and binocular perturbations. Binocular information initially is almost entirely responsible for corrections, but its relative weight decreases over time as monocular information becomes available.

Because individual subjects' data were noisy, the perturbation influence functions were derived by fitting the linear model to all of the subjects' data. To test whether the timing effects were consistent across subjects, we predicted that the timing differences apparent in Fig. 5 would result in a greater influence of binocular cue perturbations on the contact slant of the cylinder for short-duration movements than for long-duration movements. We separated each subject's trials into thirds according to duration and compared the online cue weights from the shortest-duration perturbation trials with those from the longest-duration perturbation trials. Fig. 6 shows the results of this analysis. Subjects consistently showed a larger influence of binocular perturbations for the shortest movements than for the longest movements, which matches the predictions of the model.³

3.3. Discussion

Experiment 2 had two key results: (1) subjects depended on binocular cues more than monocular cues when using online visual information to guide reaching movements, and (2) the relative influence of binocular information was higher for the online control phase than for planning. Both findings can be explained using the temporal decorrelation analysis, which showed that

³ In both experiments, subjects saw a rendered version of the cylinder come into view during the final 250–300 ms of each movement. Given that the measured sensorimotor delay was very similar to this time, specialized mechanisms for visual feedback control cannot account for the initial differences in the cue perturbation functions, which appear well before the rendered cylinder comes into view.

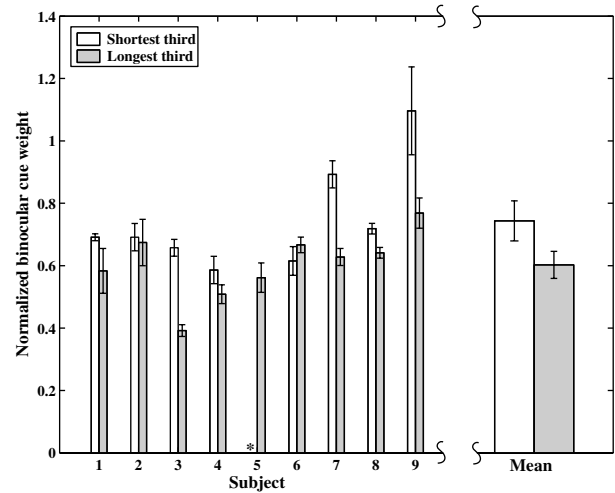


Fig. 6. Normalized binocular cue weights for the shortest- and longest-duration trials for individual subjects and averaged across subjects ($T(7) = 2.85, p < .05$). Data from Subject 5's shortest-duration movements was excluded because this subject did not show responses to the perturbations on those trials, and none of this subject's data was used to compute the means.

binocular information is processed faster than monocular information. The differences in the temporal dynamics of cue processing result in the information from binocular cues becoming available sooner than information from monocular cues, thus allowing binocular cues more time to affect movements during online control. This is consistent with our result that binocular cues had a relatively greater effect on online corrections for short-duration movements, when there was less time for monocular information to accrue, than for long-duration movements. The differences in processing speeds also help explain why binocular information dominates online control but not planning. The planning stage allowed sufficient time for information from monocular cues to accumulate, resulting in a more even balance between monocular and binocular contributions. We predict that if there were less time for planning, the temporal dynamics of cue processing would also create a bias towards binocular information during this phase.

3.3.1. Modeling

The temporal analysis suggests that while binocular cues about target surface orientation influence cumulative online corrections more than motor planning, the underlying cause appears to be a difference in the speeds at which the cues are processed. This inference is based on a comparison between the perturbation influence functions for each cue, as measured from the kinematic data. The relationship between the visual cue integration process and these influence functions, however, is indirect. Potentially, other factors in the cue integration process could give rise to similar results. Since the

conclusion suggested by the data is that the results obtained reflect differences in the temporal properties of cue processing, we must explore whether other differences between the systems processing the cues, particularly simple differences in cue reliability, could give rise to the observed patterns.

To explore this possibility, we simulated a control model that optimally integrates multiple sources of sensory information over time. Fig. 7 illustrates the structure of the model (see Appendix A for details of the model's implementation). The key element of the model is the sensory front end to the motor control system, a Kalman filter that optimally integrates incoming sensory information about surface slant from two different sensory sources. These inputs are modeled as the outputs of two low-pass temporal filters on surface slant that are perturbed by noise. The time constants of these filters determine the rate at which information from each cue accrues in the system.

The Kalman filter computes the statistically optimal estimate of target surface slant over time based on the incoming sensory information from binocular and monocular cues (Anderson & Moore, 1979). How each cue influences internal slant estimates is determined by a combination of the relative reliability of the information from each cue and the time constants of the low-pass filters associated with processing each cue. When the temporal filters associated with each cue are equivalent, the relative influence of monocular and binocular cues on the output of the filters is determined entirely by the relative uncertainties in the slant estimates derived from each. Simulations show that the relative contributions of each cue to how the filters respond to perturbations in the input remain constant over time. Differences in the time constants associated with each cue, however, in-

duce an interesting dynamic in the cue integration process. Initially, the internal estimate of slant is driven by the faster cue. When the binocular cue (assumed here to have a smaller time constant) suggests a slant that conflicts with the monocular cue, the output of the filter first tracks the slant suggested by the binocular cue, and then it slowly shifts to a more balanced estimate between the two cues. Assuming enough time has passed between stimulus presentation and motor planning, the relative influence of the two cues will reach a stable state by the time the subject initiates movement. When new information about the target stimulus arrives (when an object moves, after a saccade, or after an eye blink as simulated in the current experiment), the output of the filter initially shifts toward the slant suggested by the binocular cue but then begins to shift back toward a more balanced estimate.

The experimental data does not directly probe the internal sensory estimate of surface orientation used to guide hand movements but rather measures the output of the motor system. In order to compare model performance to human data, we coupled the output of the Kalman filter to a motor control module that mapped the internal estimate of surface orientation to rotation commands to the hand (Todorov & Jordan, 2002). We modeled a simple control law derived from the minimum jerk principle (Hoff & Arbib, 1993). The control law computes a jerk signal (third derivative of orientation) that smoothly rotates the cylinder from its current orientation toward the orientation of the target. The output of the model is the orientation of the cylinder as a function of time between the beginning of the movement and contact with the target surface.

By simulating the model under different parameter settings, we tested whether or not the empirical results

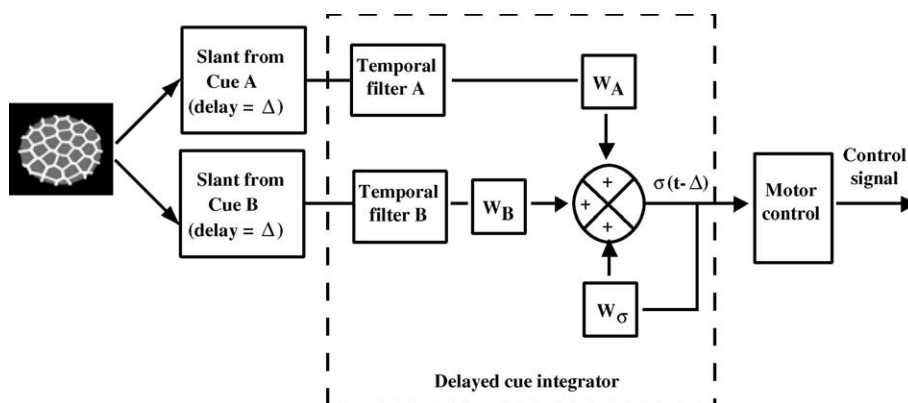


Fig. 7. A Kalman filter provides the front-end sensory mechanism for estimating target surface slant. The filter updates its internal estimate of target surface slant by combining slant estimates from binocular and monocular cues with the slant predicted from its previous internal estimate. We assume that the estimates derived from each cue are low-pass filtered. The slant estimates from each cue are combined with the running "internal" estimate of slant derived from the output of the Kalman filter using a weighted average. The weights are in proportion to their reliabilities and the reliability of the previous internal estimate. We simulated a filter that assumes the slant of the target surface can change randomly at each time step by a small amount. This causes the filter to weight new sensory information more heavily than old. The output of the system is an optimal estimate of slant from both cues. This provides input for a control model that generates a control signal for rotating the cylinder. The sensory signals are assumed to have an overall, fixed delay of Δ ms relative to the output of the motor control signal.

could be explained by one or more of three classes of models: (a) a difference in reliability of cues (no difference in processing speed), (b) a simple fixed delay in one cue relative to the other, or (c) low-pass filtering of both cues with different time constants associated with each cue. We have run a large number of simulations of the model under different parameter settings. All have shown the same qualitative behavior. This is illustrated in Fig. 8, which shows the cue influence functions computed from the outputs of specific instantiations of each of the three classes of models described above. For all simulations, we assumed a fixed sensorimotor delay of 184 ms between the output of the Kalman filter and the input to the motor control module. For the simulation shown in Fig. 8a, we assumed that the variance of the slant estimate from binocular cues was 20% lower than the variance of the slant estimate from monocular cues. For this simulation, the slant estimates derived from each cue were unfiltered. For the simulation shown in Fig. 8b, we assumed equal variance parameters but with a fixed delay of 75 ms between the output of the monocular slant estimator and the binocular slant estimator. For the final simulation shown in Fig. 8c, we filtered the outputs of the two estimators through recursive, first-order linear filters. The time constant for the monocular cue filter was 120 ms and was 8 ms for the binocular cue filter. The variance of the noise in each filter's output was adjusted so that the variances of the optimal estimators' outputs matched those from the previous two simulations.

Only the model with a difference in filter time constants could qualitatively account for the measured perturbation influence functions. The model using different cue reliabilities always gave rise to influence functions like those shown in Fig. 8a. Regardless of parameter settings, the proportional values of the cue perturbation influence functions for this model remained constant over time, which was inconsistent with the slow change present in subjects' data. Changing the delay associated with the monocular cues always gave rise to the simple shift shown in Fig. 8b. The exact shape of the perturbation influence functions was highly dependent on the uncertainty parameters and time constants associated with each cue (four free parameters). The influence functions shown in Fig. 8c were generated using a set of parameters that matched subjects' data well. Further details about the parameters used for these simulations are provided in the Appendix A.

Fig. 8 clearly shows that the low-pass filtering model gives the best qualitative match to subjects' cue perturbation influence functions. Perhaps more significant is the fact that model (a), in which only the reliabilities of the two cues differed, did not reproduce the effect that binocular cues have a stronger relative influence on total corrections for fast movements than for slow movements; it predicted that movement duration should not

affect cue influences. In contrast, with the parameters used to generate the influence functions in Fig. 8c, model (c) shows a change in the normalized binocular cue weight from 0.73 to 0.57 for the fastest and slowest movements simulated (using a range similar to the empirically observed movement times). This is almost exactly equivalent to the values measured for subjects in the experiment. The simple delay model (model (b)) shows a similar pattern. Thus, while speed-induced differences do not disambiguate the form of the temporal differences in cue processing, they clearly implicate a difference in timing.

4. General discussion

Our primary finding was that binocular cues contribute more to online control of reaching movements than to motor planning. Like Glover and Dixon (2001, 2002), we found differences between planning and online control, although our evidence does not support the existence of a functional dissociation between the perceptual processes driving these two phases. Rather, analyzing the temporal properties of the placement task showed that differences in processing speeds determine how 3D cues influence the online control phase. Binocular cues had a greater influence on online control because observers processed binocular information about surface slant more rapidly than monocular information. This seems to run counter to the common wisdom that binocular processing is slow (McKee, Levi, & Bowne, 1990). Another way to frame the result is that computing slant from monocular cues is slower than computing slant from binocular disparities, but neither is particularly fast. As in Experiment 1, reaction times to perturbations in both cues (>250 ms) were much slower than reaction times to two-dimensional target displacements. While this may reflect the more complex processing required to estimate 3D slant than to estimate 2D retinal position, it might also reflect a delay caused by the flicker mask.

The difference in processing speeds for binocular and monocular cues renders binocular cues more important for online control of hand movements, but the relative influence of the cues depends critically on movement duration. In our experiment, we used artificial blinks to mask perturbations. Another common trigger for changes in retinal information is the orienting saccade to a target (Biguer, Jeannerod, & Prablanc, 1982). In this case, the temporal dynamics of cue processing will also markedly affect the relative contributions of cues to online control of movements. The dynamics, however, may differ from what we have found here since subjects need to attain proper vergence after an orienting saccade to effectively use binocular cues. Corrections to errors in the initial conjunctive saccades are typically

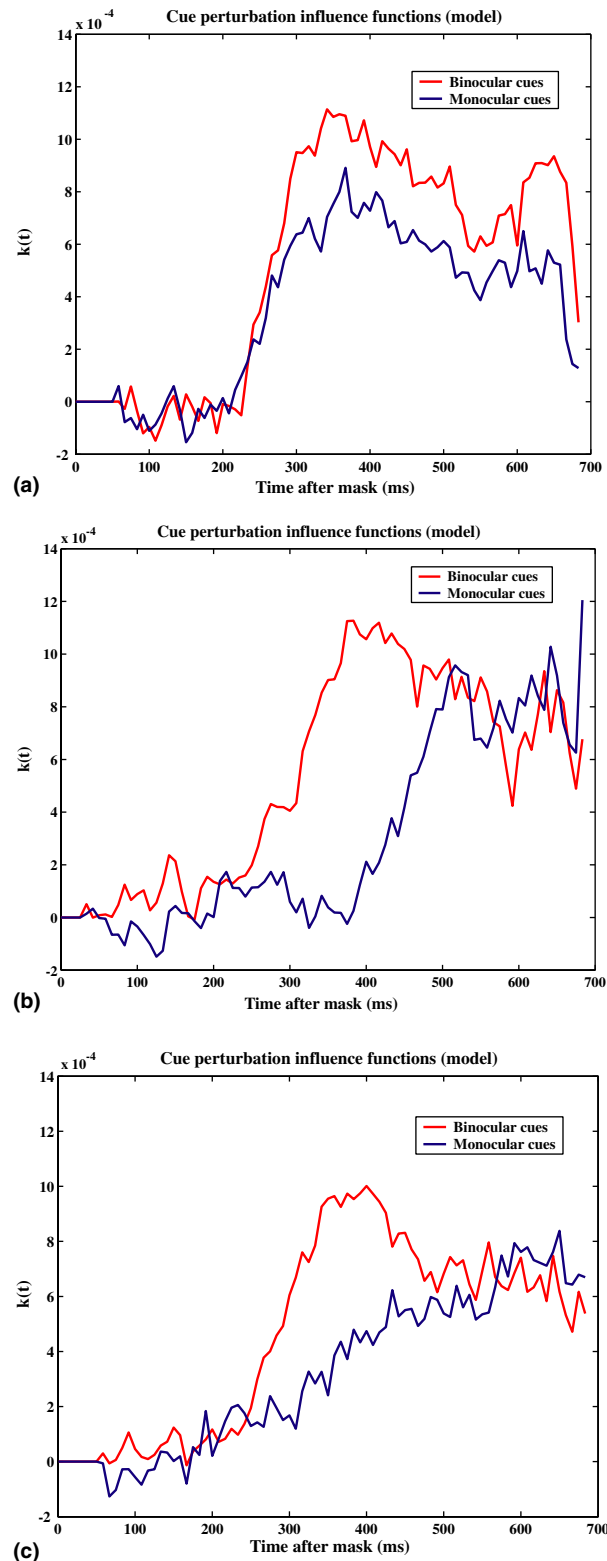


Fig. 8. Stereotypical cue perturbation functions derived from running the model in three qualitatively different sensory parameter regimes. (a) The low-pass temporal filter was a delta function impulse response (no temporal smoothing or delay), but the reliability of the monocular cues was less than that of binocular cues. (b) The filter associated with the monocular cue was assumed to be a simple delay in the output. (c) The filters associated with each cue were recursive, second-order filters that effectively smoothed and delayed the sensory estimates from each cue. Here the time constant for the monocular cue filter was significantly larger (more smoothing) than the time constant for the binocular cue filter. Details of the model parameters used for the simulations are given in the text and [Appendix A](#).

slow and smooth (van Leeuwen, Collewijn, & Erkelens, 1998), possibly slowing binocular information down to the point where monocular information begins to dominate.

Modeling the visual computations underlying natural behaviors requires fully considering the dynamics of the processes involved. The current work has revealed some features of the dynamics of 3D cue processing and shown how they can be naturally modeled using the tools of dynamic statistical estimation as embodied in the framework of Kalman filtering. Many other aspects of sensory processing are amenable to this treatment (Burgi, Yuille, & Grzywacz, 2000; Grzywacz & Hildreth, 1987; Wolpert, Ghahramani, & Jordan, 1995). For example, the model easily can be extended to deal with integrating information computed during one fixation with information derived from later fixations. Similarly, while we have considered how the visual system accrues information over time about a static stimulus, we often interact with moving stimuli. The corresponding sources of dynamic visual information (e.g. motion transients) have their own time constants, which necessarily affect how the brain uses the information for motor control. We hope that some of the tools introduced here will prove useful in studying these more complex aspects of visuomotor control.

Appendix A

The model consisted of sensory front-end for estimating target surface slant that sent its output to a motor control module for generating commands to rotate the cylinder. The sensory front-end was a Kalman filter that optimally integrated binocular and monocular information about slant over time. We modeled the motor controller as a simple kinematic controller that computed a jerk signal (third derivative of the slant of the cylinder) for adjusting the slant of the cylinder online. The instantaneous jerk signal at each time step was computed as the next step in a minimum jerk trajectory computed based on the current estimate of the slant of the target surface and of the slant of the cylinder. Slant trajectories were generated by integrating the jerk signal. Since we were interested in how constraints on sensory estimates of target surface slant impacted performance, we used a simple control system that did not use sensory feedback about the slant of the cylinder. The internal estimate of the slant of the cylinder was derived by integrating noisy versions of the jerk signal sent out by the controller. We also simulated models that incorporated sensory feedback about the slant of the cylinder, and the effects of cue perturbations about target surface slant were similar for those models.

To model the slant estimates derived from each cue, we assumed that the inputs to the Kalman filter were

independent copies of the slant suggested by each cue with added white, Gaussian noise. The slant estimates derived from each cue were low-pass filtered in time through second-order, recursive linear filters of the form

$$y(t) = \frac{t}{\tau^2} e^{-t/\tau}. \quad (\text{A.1})$$

The time constants for the filters associated with each cue were set by qualitatively matching the performance of the model to subjects' data. The internal dynamic model of the Kalman filter assumed that the slant of the target surface could change by a small amount at each time step. The state update equation for target surface slant assumed by the model was

$$\sigma(t + \delta t) = \sigma(t) + w(t), \quad (\text{A.2})$$

where $\sigma(t)$ is the slant of the surface at time t and $w(t)$ is a white noise source, and δt was set to 8 ms for our simulations.

In order to implement the low-pass filters for each cue, we augmented the state vector with a set of dummy variables that were updated with a recursive state transition matrix. Thus, we have for the state update equation for the filter,

$$X(t + \delta t) = \mathbf{A}X(t) + \Omega(t), \quad (\text{A.3})$$

where the state vector, $X(t)$, is given by

$$X(t) = \begin{bmatrix} \sigma(t) \\ \sigma'_{\text{bin}}(t) \\ \sigma''_{\text{bin}}(t) \\ \sigma'_{\text{mono}}(t) \\ \sigma''_{\text{mono}}(t) \end{bmatrix} \quad (\text{A.4})$$

and the state transition matrix, \mathbf{A} , is given by

$$\mathbf{A} = \begin{bmatrix} 1 & 0 & 0 & 0 & 0 \\ \frac{\delta t}{\tau_{\text{bin}}} & e^{-\delta t/\tau_{\text{bin}}} & 0 & 0 & 0 \\ 0 & e^{-\delta t/\tau_{\text{bin}}} & e^{-\delta t/\tau_{\text{bin}}} & 0 & 0 \\ \frac{\delta t}{\tau_{\text{mono}}} & 0 & 0 & e^{-\delta t/\tau_{\text{mono}}} & 0 \\ 0 & 0 & 0 & e^{-\delta t/\tau_{\text{mono}}} & e^{-\delta t/\tau_{\text{mono}}} \end{bmatrix}. \quad (\text{A.5})$$

Rows 2 and 3 of the state transition matrix implement the recursive low-pass filter for the estimates of slant derived from binocular cues, and rows 4 and 5 implement a similar filter for the estimates of slant derived from monocular cues. $\Omega(t)$ is a white noise process with zeros in all rows except the first. The first row is $w(t)$, the white noise process that implements the assumed random walk in surface slant.

The observed estimates of slant that serve as input to the Kalman filter are given by the equation

$$Z(t) = \mathbf{H}X(t) + \Psi(t), \quad (\text{A.6})$$

where the observation matrix \mathbf{H} is given by

$$\mathbf{H} = \begin{bmatrix} 0 & 0 & 1 & 0 & 0 \\ 0 & 0 & 0 & 0 & 1 \end{bmatrix}. \quad (\text{A.7})$$

\mathbf{H} “reads” off the outputs of the two filters, $\sigma''_{\text{bin}}(t)$ and $\sigma''_{\text{mono}}(t)$. $\Psi(t)$ is a white noise process with standard deviations representing the effective internal noise in sensory estimates of slant from each of the two cues.

The optimal estimate of target surface slant at time t is given by the Kalman update equation

$$\widehat{X}(t + \delta t) = \mathbf{A}\widehat{X}(t) + \mathbf{K}[Z(t) - \mathbf{H}\widehat{X}(t)], \quad (\text{A.8})$$

where \mathbf{K} is the Kalman gain matrix, given by

$$\mathbf{K} = \mathbf{A}\Sigma_{\widehat{X}(t)}\mathbf{H}'[\mathbf{H}\Sigma_{\widehat{X}(t)}\mathbf{H}' + \Sigma_{\Psi}]^{-1}. \quad (\text{A.9})$$

$\Sigma_{\widehat{X}(t)}$ is the error covariance matrix for the internal estimate of slant, $\widehat{X}(t)$, and Σ_{Ψ} is the covariance of the observation noise. The error covariance matrix is updated with the equation

$$\Sigma_{\widehat{X}(t)(t+\delta t)} = \Sigma_{\Omega} + \mathbf{A}\Sigma_{\widehat{X}(t)}\mathbf{A}' - \mathbf{K}\mathbf{H}\Sigma_{\widehat{X}(t)}\mathbf{A}',$$

where Σ_{Ω} is the noise covariance of the random walk process assumed for the internal estimate of surface slant.

The sensory parameters for the simulation shown in Fig. 8a were $s_w = 0.15^\circ$, $s_{\text{bin}} = 10^\circ$, $s_{\text{mono}} = 12^\circ$. The low-pass filters were not incorporated into this simulation, though doing so has no change on the pattern of results. With these parameters, the asymptotic standard deviation in the output of the filter was 1.37. The same parameters were used for the simulation of the fixed delay model shown in Fig. 8b, but with an added delay in the output of the monocular cue of 75 ms. The sensory parameters for the simulation shown in Fig. 8c, with low-pass filtering of the slant estimates derived from each cue, were $s_w = 0.15^\circ$, $s_{\text{bin}} = 14^\circ$, $s_{\text{mono}} = 160^\circ$, $\tau_{\text{bin}} = 8$ ms and $\tau_{\text{mono}} = 120$ ms. With these parameters, the asymptotic standard deviation in the output of the filter was 1.27°.

The output of the sensory model provided input to a controller that attempted to minimize the average squared jerk in movements between the current estimated slant of the cylinder and the current estimate of the slant of the target surface. Following Hoff and Arbib (1993), this is given by a controller that updates the state of the cylinder using the equation,

$$\begin{bmatrix} \sigma_{\text{cyl}}(t + \delta t) \\ \dot{\sigma}_{\text{cyl}}(t + \delta t) \\ \ddot{\sigma}_{\text{cyl}}(t + \delta t) \end{bmatrix} = \begin{bmatrix} 1 & 1 & 0 \\ 0 & 1 & 1 \\ -60/D^3 & -36/D^2 & 1 - 9/D \end{bmatrix} \times \begin{bmatrix} \sigma_{\text{cyl}}(t) \\ \dot{\sigma}_{\text{cyl}}(t) \\ \ddot{\sigma}_{\text{cyl}}(t) \end{bmatrix} + \begin{bmatrix} 0 \\ 0 \\ 60/D^3 \end{bmatrix} \hat{\sigma}(t),$$

where $\sigma_{\text{cyl}}(t)$, $\dot{\sigma}_{\text{cyl}}(t)$, and $\ddot{\sigma}_{\text{cyl}}(t)$ are the slant of the cylinder at time t and its first and second derivatives, and $\hat{\sigma}(t)$ is the perceptual estimate of the slant of the target surface. D is the time remaining in the movement.

We simulated the model for 1000 trials using the same perturbation conditions used in Experiment 2. To match the variance in subjects' movement durations, we randomly chose the total movement duration on each trial from a uniform distribution between 650 and 1000 ms. To simulate the measurement error in the slants derived from the Optotrak recordings (derived from sample variances in the measured slant of a stationary cylinder), we added white Gaussian noise with a standard deviation of .0125° (an estimate derived from the standard deviation in slant measurements taken from a stationary cylinder) to the slant trajectories generated by the model. We then analyzed the resulting “measured” slant trajectories to compute cue perturbation functions for the model, as shown in Fig. 8.

References

- Anderson, B. D. O., & Moore, J. B. (1979). Optimal filtering. *Prentice-Hall information and system sciences series* (p. 357). Englewood Cliffs, NJ: Prentice-Hall.
- Biguer, B., Jeannerod, M., & Prablanc, C. (1982). The coordination of eye, head, and arm movements during reaching at a single visual target. *Experimental Brain Research*, *46*(2), 301–304.
- Burgi, P. Y., Yuille, A. L., & Grzywacz, N. M. (2000). Probabilistic motion estimation based on temporal coherence. *Neural Computation*, *12*(8), 1839–1867.
- Desmurget, M., Prablanc, C., Arzi, M., Rossetti, Y., Paulignan, Y., & Urquizar, C. (1996). Integrated control of hand transport and orientation during prehension movements. *Experimental Brain Research*, *110*, 265–278.
- Ernst, M. O., & Banks, M. S. (2002). Humans integrate visual and haptic information in a statistically optimal fashion. *Nature*, *415*(6870), 429–433.
- Glover, S. R., & Dixon, P. (2001). Dynamic illusion effects in a reaching task: Evidence for separate visual representations in the planning and control of reaching. *Journal of Experimental Psychology-Human Perception and Performance*, *27*(3), 560–572.
- Glover, S. R., & Dixon, P. (2002). Dynamic effects of the Ebbinghaus illusion in grasping: Support for a planning/control model of action. *Perception and Psychophysics*, *64*(2), 266–278.
- Goodale, M. A., Pelisson, D., & Prablanc, C. (1986). Large adjustments in visually guided reaching do not depend on vision of the hand or perception of target displacement. *Nature*, *320*(6064), 748–750.
- Grzywacz, N. M., & Hildreth, E. C. (1987). Incremental rigidity scheme for recovering structure from motion—position-based versus velocity-based formulations. *Journal of the Optical Society of America A-Optics Image Science and Vision*, *4*(3), 503–518.
- Hillis, J. M., Ernst, M. O., Banks, M. S., & Landy, M. S. (2002). Combining sensory information: Mandatory fusion within, but not between, senses. *Science*, *298*(5598), 1627–1630.
- Hillis, J. M., Watt, S. J., Landy, M. S., & Banks, M. S. (2004). Slant from texture and disparity cues: Optimal cue combination. *Journal of Vision*, *4*(12), 967–992.
- Hoff, B., & Arbib, M. A. (1993). Models of trajectory formation and temporal interaction of reach and grasp. *Journal of Motor Behavior*, *25*(3), 175–192.

- Jacobs, R. A. (1999). Optimal integration of texture and motion cues to depth. *Vision Research*, 39(21), 3621–3629.
- Knill, D. C., & Kersten, D. (2004). Visuomotor sensitivity to visual information about surface orientation. *Journal of Neurophysiology*, 91(3), 1350–1366.
- Knill, D. C., & Saunders, J. A. (2003). Do humans optimally integrate stereo and texture information for judgments of surface slant?. *Vision Research*, 43(24), 2539–2558.
- Landy, M. S., Maloney, L. T., Johnston, E. B., & Young, M. (1995). Measurement and modeling of depth cue combination—in defense of weak fusion. *Vision Research*, 35(3), 389–412.
- McKee, S. P., Levi, D. M., & Bowne, S. F. (1990). The imprecision of stereopsis. *Vision Research*, 30(11), 1763–1779.
- Paulignan, Y., Jeannerod, M., Mackenzie, C., & Marteniuk, R. (1991). Selective perturbation of visual input during prehension movements. 2. The effects of changing object size. *Experimental Brain Research*, 87(2), 407–420.
- Paulignan, Y., Mackenzie, C., Marteniuk, R., & Jeannerod, M. (1991). Selective perturbation of visual input during prehension movements. 1. The effects of changing object position. *Experimental Brain Research*, 83(3), 502–512.
- Pelisson, D., Prablanc, C., Goodale, M. A., & Jeannerod, M. (1986). Visual control of reaching movements without vision of the limb. 2. Evidence of fast unconscious processes correcting the trajectory of the hand to the final position of a double-step stimulus. *Experimental Brain Research*, 62(2), 303–311.
- Prablanc, C., & Martin, O. (1992). Automatic-control during hand reaching at undetected 2-dimensional target displacements. *Journal of Neurophysiology*, 67(2), 455–469.
- Saunders, J. A., & Knill, D. C. (2001). Perception of 3D surface orientation from skew symmetry. *Vision Research*, 41(24), 3163–3183.
- Saunders, J. A., & Knill, D. C. (2003). Humans use continuous visual feedback from the hand to control fast reaching movements. *Experimental Brain Research*, 152(3), 341–352.
- Saunders, J. A., & Knill, D. C. (2004). Visual feedback control of hand movements. *Journal of Neuroscience*, 24(13), 3223–3234.
- Soechting, J. F., & Lacquaniti, F. (1983). Modification of trajectory of a pointing movement in response to a change in target location. *Journal of Neurophysiology*, 49(2), 548–564.
- Todorov, E., & Jordan, M. I. (2002). Optimal feedback control as a theory of motor coordination. *Nature Neuroscience*, 5(11), 1226–1235.
- van Leeuwen, A. F., Collewyn, H., & Erkelens, C. J. (1998). Dynamics of horizontal vergence movements: Interaction with horizontal and vertical saccades and relation with monocular preferences. *Vision Research*, 38(24), 3943–3954.
- Wolpert, D. M., Ghahramani, Z., & Jordan, M. I. (1995). An internal model for sensorimotor integration. *Science*, 269(5232), 1880–1882.